

1 **Synergistic retrievals of ice in high clouds from lidar, Ku-band radar and**
2 **submillimeter wave radiometer observations**

3 Mircea Grecu^a and John Yorks ^a

4 ^a *NASA GSFC*

5 *Corresponding author:* Mircea Grecu, mircea.grecu-1@nasa.gov

⁶ ABSTRACT: Enter the text of your abstract here.

7 1. Introduction

8 The future NASA Atmospheric Observing System (AOS) mission (Braun 2022) is expected to
9 feature new combinations of observations that may be used to quantify the amounts of ice in high
10 clouds and characterize the microphysical properties of ice particles. These observations include
11 lidar backscatter, Ku-band radar reflectivity and submillimeter wave radiometer brightness tem-
12 perature measurements. While not optimal for cloud ice estimation, but for the characterization
13 of a broader spectrum of cloud and precipitation processes, these observations are nevertheless
14 synergistic from the characterization of ice clouds perspective. That is, despite the fact that lidar
15 observations attenuate quickly in thick ice clouds and the Ku-band radar will not be able to de-
16 tect clouds characterized by an echo weaker than 8.0 dBZ, the active observations are expected
17 to provide context that may be incorporated into radiometer retrievals. In this study, we inves-
18 tigate the impact of incorporating the lidar and radar observations into the radiometer retrieval
19 of ice clouds. Because the existent amount of coincident backscatter lidar, Ku-band radar, and
20 submillimeter-wave radiometer observations is rather insufficient to derive conclusive results, we
21 employ accurate physical models to simulate the lidar, radar and radiometer observations and use a
22 cross-validation methodology to characterize the retrieval accuracy. As retrievals from passive in-
23 strument observations strongly depend on the "a priori" information (Rodgers 2000), for the results
24 to be relevant in real applications it is necessary to base them on realistic vertical distributions of
25 ice properties. Such distributions may be derived from cloud-resolving-model (CRM) simulations
26 (Pfreundschuh et al. 2020) or directly from observations. In this study, we employ the latter
27 approach, as CRMs may still be deficient in properly reproducing the vertical distribution of ice
28 clouds and their associated microphysical properties. Specifically, we use observation and products
29 from the CloudSat (CS) mission (Stephens et al. 2002) to derive a database of ice microphysical
30 properties and associated simulated lidar, radar and radiometer observations. The database is used
31 to investigate the accuracy of the retrieved ice cloud properties from the simulated observations.
32 The article is organized as follows. In Section 2, we describe the approach used to derive the ice
33 properties and the associated simulated observations, the retrieval and the evaluation methodology.
34 In Section 3, we present the results of the evaluation methodology. We conclude in Section 4.

35 **2. Methodology**

36 As previously mentioned, we use CloudSat (CS) observations (Stephens et 2002) to derive the
37 vertical distributions of ice properties needed in the investigation. Although research quality CS
38 cloud ice products exist, to maximize the physical consistency of the approach, we do not use them
39 but derive ice amounts and associated properties directly from CS reflectivity observations. This
40 ensures the consistency between the particle distribution assumptions and the electromagnetic
41 scattering properties used in the CS reflectivity processing and those used the simulation of
42 the lidar, Ku-band radar and radiometer observations. Lidar, Ku-band radar and submillimeter-
43 wave radiometer observations are simulated from CS observations using accurate physical models
44 and realistic assumptions consistent with the most recent knowledge in the field of ice cloud
45 microphysics, and a non-parametric estimation methodology based on the k-Means clustering
46 algorithm MacKay (2003) is used to investigate the instrument synergy. Details of the methodology
47 are presented below.

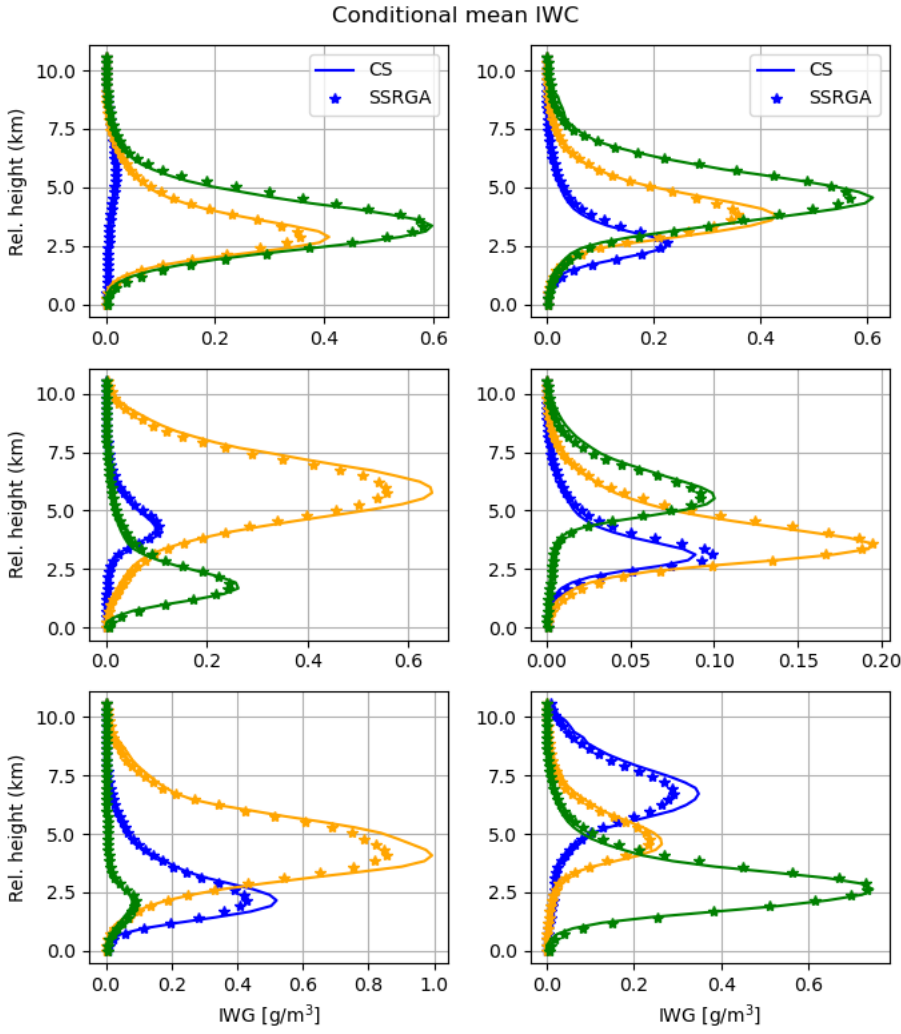
48 *a. Assumptions and forward models*

49 To quantify the number of ice particles in an elementary atmospheric volume as a function of
50 their size, we use normalized gamma functions (Bringi et al. 2003). The benefit of normalized
51 gamma functions is that they encapsulate the variability of Ice Water Content (IWC) - reflectivity
52 relationship into a single parameter, i.e. the normalized Particle Size Distribution (PSD) intercept
53 (Testud et al. 2001; Bringi et al. 2003). The normalized PSD intercept is defined as $N_w = \frac{4^4}{\pi \rho_w} \frac{IWC}{D_m^4}$,
54 where IWC is the ice water content associated with the PSD, and D_m is the mass weighted mean
55 diameter. Testud et al. (2001) showed that the variability in IWC reflectivity (Z) relationships may
56 be fully explained by variability in N_w , and that a formula of the type

$$IWC = N_w^{1-b} a Z^b \quad (1)$$

61 perfectly explains the relationships between IWC and Z calculated from observed PSDs. Equation
62 (1) is not sufficient to derive accurate, unbiased estimates of ice water contents, because N_w
63 varies considerably in time and space. Nevertheless, multiple studies showed that it is beneficial
64 to parameterize N_w as a function of various variables, such as temperature (e.g. Hogan et al.

2006; Delanoe and Hogan 2008; Deng et al. 2010), rather than using N_w independent relations.
In this study, we parameterize N_w as a function of temperature based on the CloudSat 2C-ICE
product (Deng et al. 2010; Deng et al. 2013). Specifically, we cluster, based on similarity, a
large set 2C-ICE profiles into 18 classes using a k-Means procedure. The mean IWC profiles
associated with the 18 classes are shown in continuous lines in Figure 1. Alternative estimates,
derived using PSD assumptions and electromagnetic scattering calculations that enable accurate
and physically consistent simulations of radar observations at Ku-band and radiometer observations
of submillimeter-wave frequencies are also shown in Figure 1. These estimates are based on the
self-similarity Rayleigh-Gans approximation (SSRGA) of Hogan et al. (2017). Details regarding
the estimation process are provided in the following paragraphs. As apparent in Figure 1, the CS
and SSRGA estimates are in good agreement. Some discrepancies due to differences between
the SSRGA N_w parameterization and the CS 2C-ICE "a priori assumptions" are also apparent,
but they are not deemed critical in this study, whose objective is the investigation of synergistic
lidar, Ku-band radar and submillimeter-wave radiometer retrievals, because the outcome is not
likely to be sensitive to such details. One may notice that the average IWC profiles in Figure 1
are characterized by different peak values and heights. This facilitates a simple way to reverse-
engineer to (some extent) the "a priori" assumptions used in the CS 2C-ICE product and use them
in formulation of the type described in Equation (1). Specifically, the derivation of relationships
of the type $IWC = a_i Z^{b_i}$ for every class i may be used to study a_i as a function of height. Shown
in Figure 2 is a representation of the class multiplicative coefficient a_i as a function of relative
height scatter plot. As apparent in the figure, and as expected, a_i exhibits a strong variation with
the relative height. Coefficient b_i exhibits a height dependency as well (not shown), but the range
of variation is significantly smaller, almost zero relative to the mean value of b . Given that any
deviation of the multiplicative coefficient in an IWC-Z relation from an average is equivalent to a
deviation of the associated N_w from its mean value (Testud et al. 2001), the variation of a as a
function of relative-height may be converted into a N_w as a function of relative-height relationship.
We, therefore, use the data in Fig. 2 to parameterize N_w as a function of the relative height.
For the determination of reference a and b values to be used with Equation (1), we assume that
PSDs are normalized gamma distributions with $N_w = 0.08 cm^{-4}$ and $\mu = 2$ and calculate



57 FIG. 1. Mean CS IWC profiles for 18 classes derived using the k-Means clustering algorithm. Associated
 58 mean profiles derived from CS reflectivity observations derived using SSRGA scattering calculations and N_w
 59 parameterization developed in this study are shown using symbol *. The vertical coordinate is defined relative
 60 to the freezing level

$$Z = \frac{\lambda^4}{\pi^5 |K_w|^2} \int_0^\infty N(D, D_m) \sigma_b(D) dD \quad (2)$$

94 where λ is the radar frequency, $|K_w|$ is the dielectric factor of water, $N(D, D_m)dD$ is the number
 95 of ice particles of diameter with D and $D+dD$ per unit volume, D_m is the mass weighted mean
 96 diameter of the distribution, and $\sigma_b(D)$ is the backscattering cross-section of ice particle of

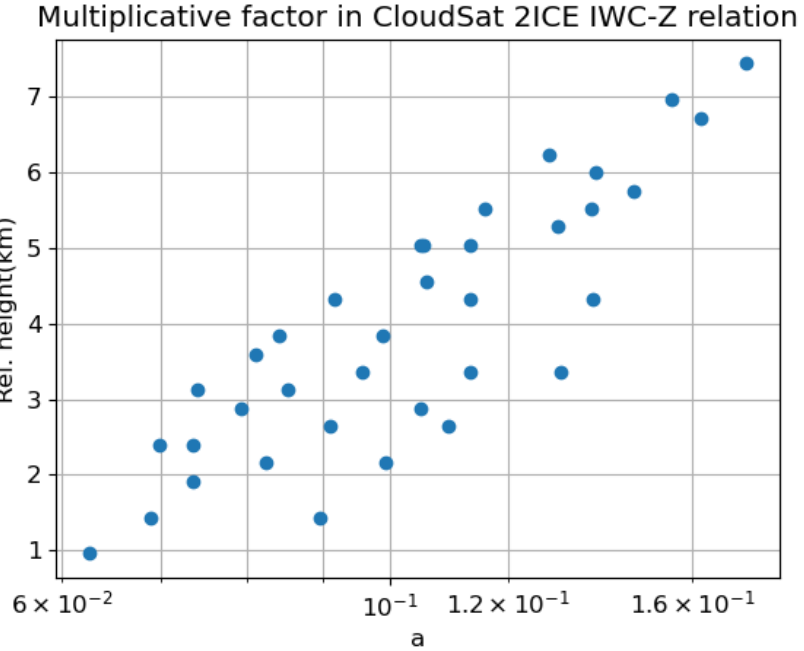
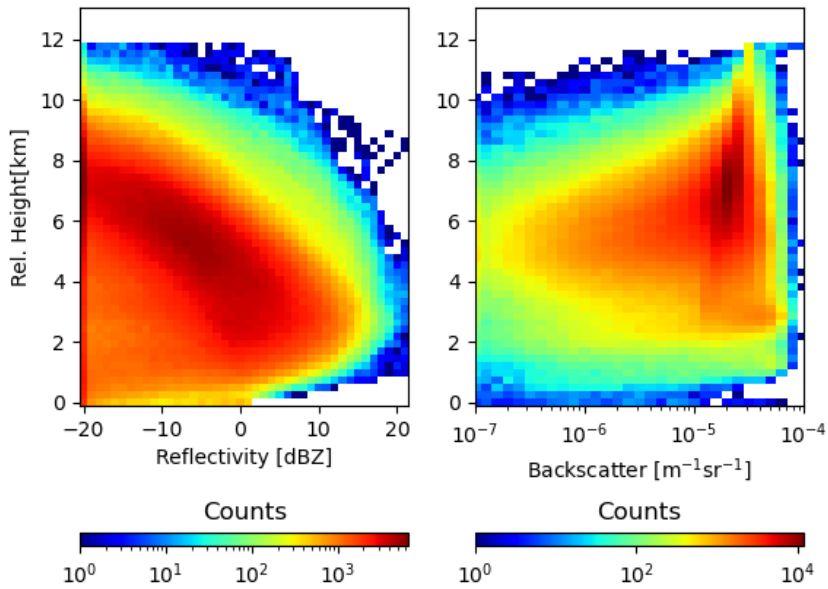


FIG. 2.

diameter D . The mass weighted mean diameter is equidistantly sampled to span the entire range of IWC values in the CS 2C-ICE dataset. The assumed mass-size relation is that of Brown and Francis (1995) because it works well with the SSRGA scattering calculations (Heymsfield et al. 2022). The open source software scatter-1.1 of Hogan (2019) is used to provide the actual scattering properties. The SSRGA theory was developed for millimeter and submillimeter-wave calculations and may not be applicable at lidar's wavelength. Therefore, for lidar calculations, we use the Mie solution included in the scatter-1.1 package. Although more accurate calculations based on more realistic ice particle shapes exist, they are rather incomplete and not readily available. Moreover, Wagner and Deleny (2022) compared lidar backscatter observations with backscatter calculations based on coincident PSD observations and the Mie solution and found good agreement, which suggests that electromagnetic properties derived from Mie calculations are adequate for practical applications. The lidar molecular backscatter and extinction are calculated using the lidar module of the CFMIP Observation Simulator Package (COSP; Bodas-Salcedo et al. 2011). To account for multiple-scattering in the lidar observations, we are using the multiscatter-1.2.11 model (Hogan 2015) of Hogan and Battaglia (2008). Shown in Figure 3 are the distributions of simulated Ku-band radar reflectivity and lidar bacscat as function of height above the freezing level.



113 FIG. 3. Simulated distributions of Ku-band radar reflectivity (left) and lidar backscatter (right) as function of
 114 height above the freezing level

115 The radiometer observations are calculated using a one-dimensional efficient, but accurate,
 116 radiative transfer solver based on Eddington's approximation (Kummerow 1993). The Eddington's
 117 approximation has been found to work well in cloud and precipitation retrieval application despite
 118 its simplicity relative to more general (but also computationally intensive) approaches such as the
 119 Monte Carlo radiative transfer solvers (Liu et al. 1996). It should be noted though that the phase
 120 functions of ice particles tend to be highly asymmetric at sub-millimeter wave frequencies. For
 121 radiative transfer solutions based on the Eddington's approximation to be accurate it is necessary that
 122 the delta-scaling approach (Joseph et al. 1976) be employed. The delta-scaling approach transforms
 123 the initial radiative transfer equation into an equivalent one characterized by a less asymmetric
 124 scattering function and more extinction, which makes the solution Eddington approximation more
 125 stable and accurate. The absorption due to water vapor and other gases is quantified using the
 126 Rosenkranz model (Rosenkranz 1998). The water vapor, temperature and pressure distributions
 127 are derived based on a WRF simulation of summer convection over the United States. Specifically,
 128 the water vapor, temperature and pressure profiles associated with times and areas where the

model produces anvils are selected and clustered into 40 classes using the k-Means approach. The mean extinction profiles at the radiometer frequencies are calculated for every class and used in process of calculating the brightness temperatures from the estimated ice profiles using a simple Monte Carlo procedure. That is, given a retrieved ice profile and its scattering property, an anvil class and its associated absorption, temperature and pressure profiles are randomly selected and attached to the ice scattering properties. To make the procedure physically meaningful, temperature rather than height is used in the ice scattering-gas absorption collocation process. The emissivities are randomly chosen between 0.8 and 1.0 and assumed constant for all radiometer frequencies. Brightness temperatures are calculated at 89-, 183.31 ± 1.1 , and 325.15 ± 1.5 GHz, which correspond to three of the 10 channels of the SAPHIR-NG radiometer envisioned to be deployed in the AOS mission (Brogniez et al. 2022). The other channels are centered on the same water vapor absorption lines and are not likely to offer additional information in this rather controlled experiment. Nevertheless, the other channels are expected to be useful in reducing the uncertainties caused by variability in the vertical distribution of water vapor, which may be greater in real life than in the simulated environment.

The processing steps used to process the CS reflectivity observations and calculate the lidar, Ku-band and submillimeter-wave radiometer observations may be summarized as follows:

1. Derivation of physically consistent radar and radiometer lookup tables to relate basic radar and radiometer properties (e.g. reflectivity, attenuation, extinction, scattering-albedo, etc.) to PSD parameters such as IWC and D_m . The tables are derived for a single of N_w , but are usable with any value of N_w using the "normalization" operations described in Grecu et al. (2011).
2. Derivation of Nw-relative height parameterization using the 2C-ICE product.
3. Estimation of IWC and related PSD parameters from CS W-band radar observations, using the tables constructed in Step 1 and parameterization derived in Step 2.
4. Calculation of lidar, Ku-band radar and radiometer observations from the estimates derived in Step 3 and the tables obtained in Step 1.

156 The application of these steps produces a large dataset of approximately 200,000 cloud ice
157 profiles and associated lidar, radar and radiometer observations that may be used to investigate the
158 synergy of the three sensors. Details are provided in the next section.

159 *b. Estimation and evaluation*

160 Given that the lidar observations may attenuate quickly in thick clouds, while the Ku-band radar
161 will not detect clouds with an echo weaker than 8.0 dBZ, the radiometer is the instrument likely
162 to provide by itself the most complete information about the total amount of ice in its observing
163 volume. However, the vertical distribution of ice is difficult to quantify from radiometer-only
164 observations, because significantly different ice vertical distributions may lead to very similar
165 radiometer observations. This makes radiometer-only retrievals highly dependent on the "a priori"
166 information on the distribution of ice clouds in the atmosphere. As previously mentioned, this
167 is the reason why CS-based IWC retrievals were preferred to CRM simulations, as retrievals are
168 expected to exhibit more natural and less biased distributions.

169 We employ a two-step estimation methodology similar to that of Grecu et al. (2018). In the first
170 step, we estimate from the simulated observations the IWC class, out of the 18 classes of shown
171 in Figure 1, to which the estimated IWC profile is most likely to belong. In the second step, we
172 estimate the IWC profile, using a class specific ensemble Kalman Smoother (EKS) methodology
173 similar to that of Grecu et al. (2018). The EKS algorithm updates the estimated IWC relative to
174 the mean IWC of the class to which the profile belongs based on the differences between the actual
175 active and passive observations and their mean class values. The second step of this procedure is
176 formally identical to the one used in Grecu et al. (2018), but the first step is different. In Grecu
177 et al. (2018), the first step was based on a simple distance-based evaluation. That strategy is
178 likely to be suboptimal in this study, because the joint distribution of IWC profiles and associated
179 observations are significantly more complex. We therefore use a more complex classification
180 methodology based on the TensorFlow library (Abadi et al. 2016). The class estimation model is
181 defined as a TensorFlow Model with two dense layers of 30 neurons each, followed by a softmax
182 layer (Goodfellow et al. 2016). The class estimation model is trained using the 70% of the simulated
183 observations and the corresponding IWC profiles, the remaining 30% of the data being used for
184 evaluation.

$$\mathbf{X} = \bar{\mathbf{X}}_i + \mathbf{Cov}(\mathbf{X}_i, \mathbf{Y}_i) \mathbf{Cov}(\mathbf{Y}_i, \mathbf{Y}_i)^{-1} (\mathbf{Y} - \bar{\mathbf{Y}}_i) \quad (3)$$

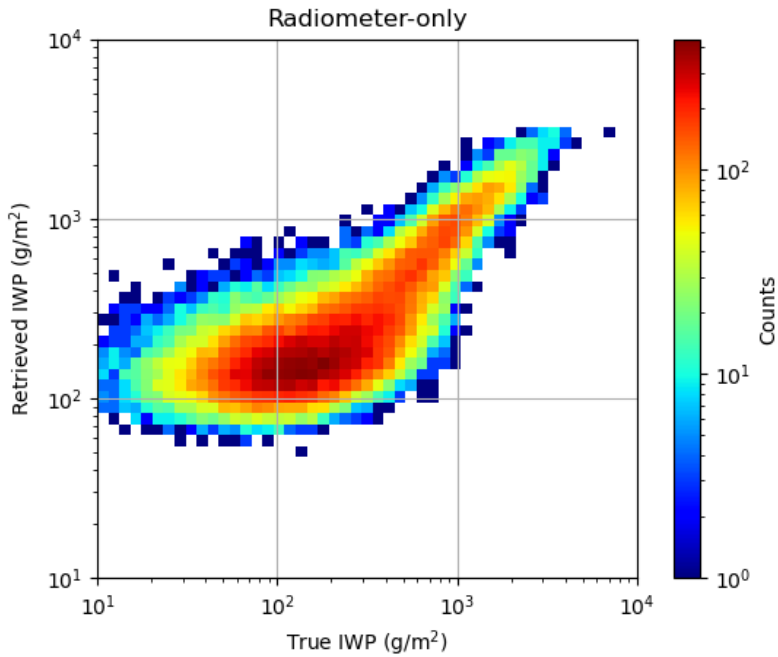
where \mathbf{X} is the state variable describing the IWC profile, \mathbf{Y} is the vector containing the variation, \mathbf{X}_i is the set of state variables for profiles in class i , and \mathbf{Y}_i is the set of associated observations. Variables $\bar{\mathbf{X}}_i$ and $\bar{\mathbf{Y}}_i$ are the mean values of the state variables and observations in class i , respectively. The covariance matrices between \mathbf{X}_i and \mathbf{Y}_i are denoted by $\mathbf{Cov}(\mathbf{X}_i, \mathbf{Y}_i)$. In step 1, the class is estimated using the TensorFlow model, while in step 2, the IWC profile is estimated using the EKS algorithm summarized in Equation 3.

As already mentioned, a cross validation methodology is used for evaluation, with 70% of the data used for training and the remaining 30% of the data used for validation. The partition of the data into training and evaluation subsets is done randomly. Usually, the partition, training and evaluation steps are repeated several times. However, given the fact that differences in the relationships between the ice property and their associated simulated observations are functions of the meteorological context, and that all regimes are well-sampled in both the training and testing subsets (e.g. out of every 10 pixels in a scene, about 7 end-up in the training dataset, while the others in the testing dataset), the repetition of the partition, training, and evaluation steps multiple times is not necessary. Therefore, in our evaluation, we partition the data into training and evaluation only once and perform all the evaluation for a single partition. The evaluation criteria include the correlation coefficient, the bias, and visual inspections of graphical representations of the estimated properties relative to their references.

3. Results

a. Radiometer-only retrievals

As previously mentioned, submillimeter-wave radiometers are likely to provide by themselves more complete information about the total amount of ice in their observing volumes than lidars or Ku-band radars with limited sensitivity. However, radiometers observations are an integrated measure of radiative process in clouds that provide little information about the vertical distribution of ice. From this perspective, an evaluation in terms of the ice water path (IWP) defined as the vertical integral of the IWC , i.e. $IWP = \int_0^{Z_{top}} IWC(z) dz$ is insightful. Shown in Figure 4 is the



205 FIG. 4. Frequency plot of estimated IWP derived radiometer-observations as a function of the true IWP used
206 in observations synthesis

213 frequency of IWP estimated from radiometer-only observations as a function of its true value. As
214 apparent in the figure, there is good correlation between the retrieved and the true IWP values.
215 The numerical value of the correlation coefficient is 0.92, and there is no-overall bias. That is, the
216 mean values of retrieved *IWP* and true *IWP* values are equal. However, conditional biases are
217 apparent, with overestimation of *IWP* for values smaller than 100 g/m^2 and some underestimation
218 for values larger than 1000 g/m^2 . The biases at the low end of the *IWP* range are not surprising,
219 given that the impact caused by ice scattering on the total radiometric signal is small for low
220 values of *IWP* and hard to distinguish from other sources of variability in radiometer observations.
221 Saturation effects are most likely responsible for underestimation at the high end. It should be
222 noted that in this evaluation, only atmospheric profiles that exhibit ice detectable by the CS radar
223 are used. Therefore, a radiometer-only estimation procedure derived from this training dataset
224 is likely to result in significant overestimation if not used in conjunction with a discrimination
225 procedure. However, such procedure is not critical in this study, as the lidar observations may be
226 used to discriminate between clear skies and ice clouds. Although the radiometer-only estimation

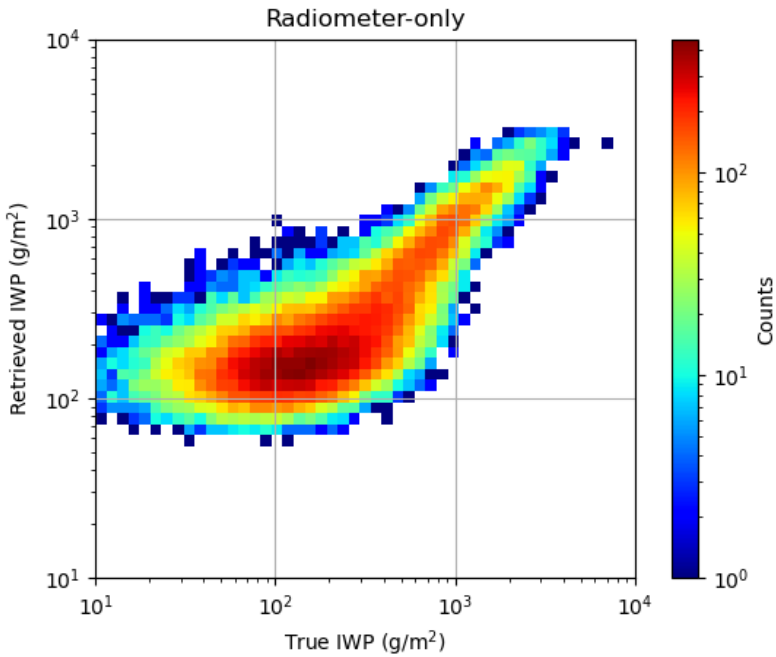


FIG. 5. True and radiometer-only retrieved conditional mean IWC for the 18 classes described in Figure 1.

procedure is able to estimate the integrated amount of ice in clouds fairly well, its ability to characterize the vertical distribution of ice in clouds is limited. Figure 5 shows the conditional vertical distributions of the estimated and true IWC for the 18 classes described in Section 2a and shown in Figure 1. As apparent in the figure, there are significant differences between the estimated and true IWC profiles.

Further insight into the radiometer-only estimation performance may be derived by defining the ice profile gravity center (GC) as $z_{GC} = \frac{\int_0^{Z_{top}} z IWC(z) dz}{\int_0^{Z_{top}} IWC(z) dz}$, where z is the distance relative to the freezing level, the Z_{top} is the distance from the top of the atmosphere to the freezing level. Shown in Figure 6 is the frequency of IWC gravity center estimated from radiometer-only observations as a function of its true value. It may be observed in the figure that while the true IWC gravity center exhibits quite a broad distribution, the one retrieved from the radiometer-only observations exhibits a multimodal narrow distribution. Moreover, there is almost no correlation between the retrieved and the true IWC gravity center. This is another indication that, while the total amount of ice may be reasonably estimated from radiometer-only observations, its vertical distribution can not be determined from radiometer-only observations.

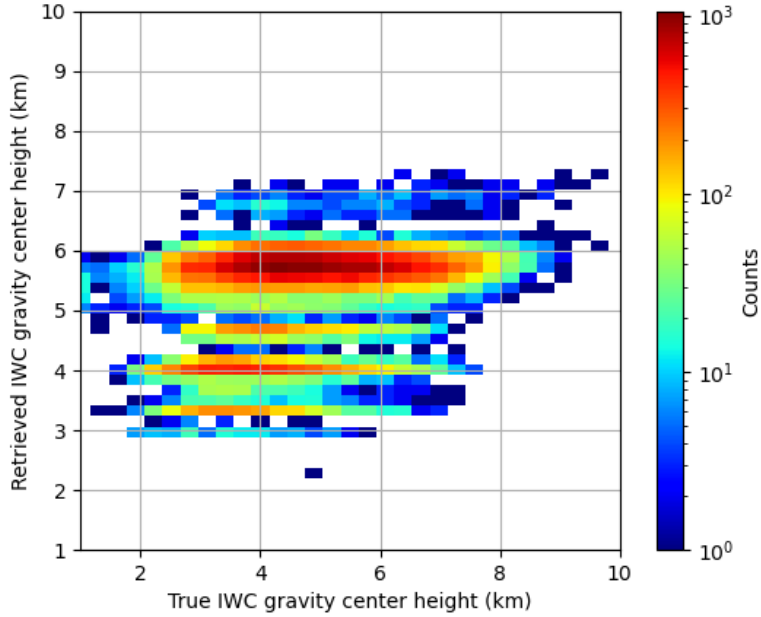


FIG. 6. Same as in Figure 3, but for the *IWC* gravity center.

b. Synergistic retrievals

From the synergy of the instrument perspective, it is useful to investigate how information easily derivable from the active instrument observation can complement the submillimeter-wave radiometer observations. The top of the clouds derived from the lidar backscatter observations is such information. To incorporate it into the *IWC* retrievals, we simply extend the dimension of the input by one entry that contains the lidar-based cloud top estimate. This additional piece of information makes the retrievals more specific by confining the set of potential matches to those that are consistent from the cloud top perspective with the lidar observations.

Shown in Figure 5 is frequency plot of the *IWC* gravity centers estimated from lidar and radiometer observations as a function of the true *IWC* gravity centers. One may note in the figure a significant improvement relative to Figure 4.

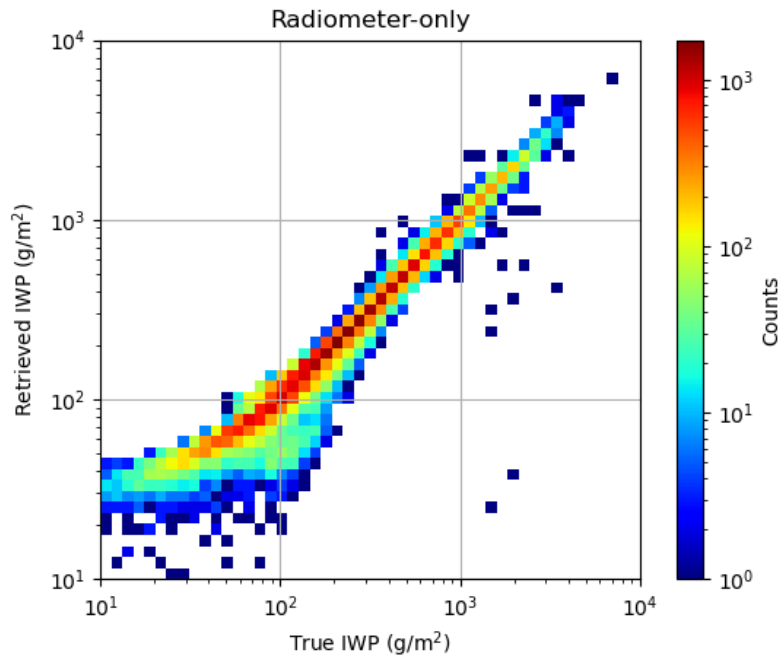


FIG. 7. .

TABLE 1. Performance summary.

Instruments				
Score	Radiometer	Radar-Radiometer	Lidar-Radiometer	Radar-Lidar-Radiometer
NRMS	0.73	0.59	0.32	0.22
Class. Accuracy	0.39	0.48	0.92	0.94

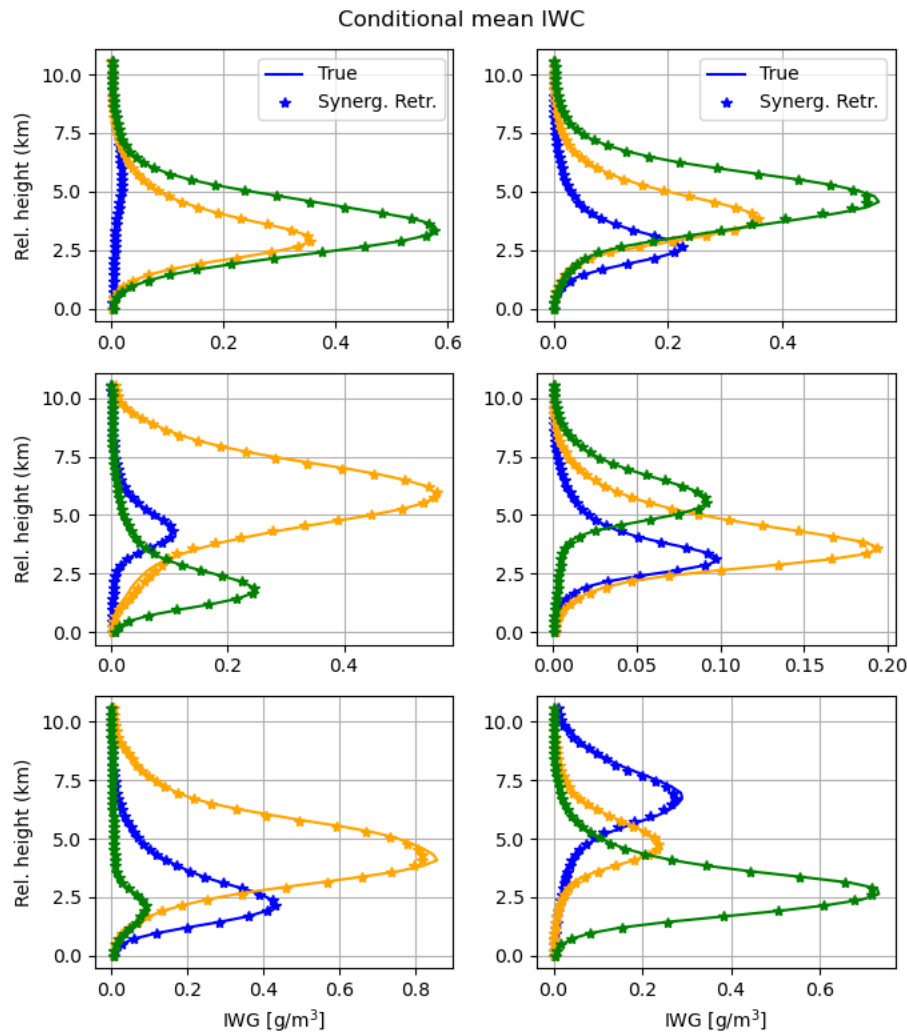


FIG. 8. .

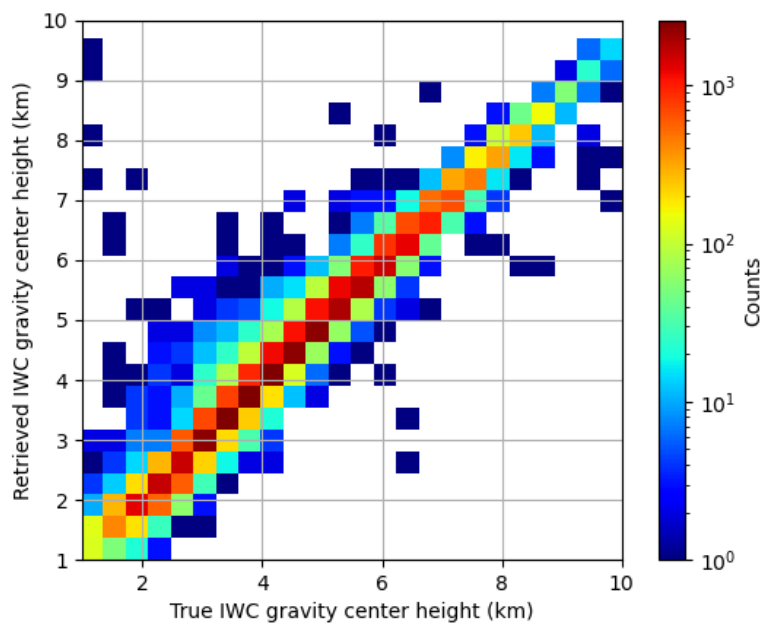


FIG. 9. .

253 *Acknowledgments.*

254 *Data availability statement.*

255 **References**

- 256 Abadi, M., and Coauthors, 2016: Tensorflow: a system for large-scale machine learning. *Osdi*,
257 Savannah, GA, USA, Vol. 16, 265–283.
- 258 Goodfellow, I., Y. Bengio, and A. Courville, 2016: *Deep learning*. MIT press.
- 259 Grecu, M., L. Tian, G. M. Heymsfield, A. Tokay, W. S. Olson, A. J. Heymsfield, and A. Bansemer,
260 2018: Nonparametric methodology to estimate precipitating ice from multiple-frequency radar
261 reflectivity observations. *Journal of Applied Meteorology and Climatology*, **57** (11), 2605–2622.
- 262 MacKay, D. J., 2003: *Information theory, inference and learning algorithms*. Cambridge university
263 press.